

See discussions, stats, and author profiles for this publication at: <https://www.researchgate.net/publication/215696023>

# Neutral Tantalum–Carbide Clusters: A Multiphoton Ionization and Density Functional Theory Study

ARTICLE *in* THE JOURNAL OF PHYSICAL CHEMISTRY A · APRIL 2000

Impact Factor: 2.69 · DOI: 10.1021/jp993489v

---

CITATIONS

25

---

READS

33

## 4 AUTHORS, INCLUDING:



**Michael William Heaven**

Department of Economic Development, Jobs...

27 PUBLICATIONS 925 CITATIONS

SEE PROFILE



**Mark A. Buntine**

Curtin University

108 PUBLICATIONS 1,412 CITATIONS

SEE PROFILE



**Gregory F Metha**

University of Adelaide

81 PUBLICATIONS 824 CITATIONS

SEE PROFILE

# Neutral Tantalum–Carbide Clusters: A Multiphoton Ionization and Density Functional Theory Study

Michael W. Heaven, Gerarda M. Stewart, Mark A. Buntine, and Gregory F. Metha\*

Department of Chemistry, The University of Adelaide, South Australia 5005, Australia

Received: September 29, 1999; In Final Form: December 21, 1999

Neutral tantalum–carbide clusters,  $Ta_mC_n$  ( $m = 1–6$ ,  $n = 1–7$ ), have been formed in a supersonic expansion following the reaction of tantalum and acetylene in a laser ablation source. These clusters have been subjected to multiphoton ionization at 532 and 355 nm and the mass spectra recorded in a reflectron time-of-flight mass spectrometer. The cluster distributions show a drop off after  $m = 4$  suggesting the stabilization of clusters containing four tantalum atoms. We have investigated the structures of these clusters using density functional theory and shown that the smaller clusters tend to form fragments of face-centered cubes, culminating in the formation of a distorted cube of stoichiometry  $Ta_4C_4$ . The structure of  $Ta_4C_4$  is shown to be a distorted tetrahedron, or “butterfly”, made up of four tantalum atoms with a carbon atom bonded to each face. The theoretical calculations also indicate that clusters containing three tantalum atoms form a triangle and that there is competition for the carbon atoms to bond to either the face or the edge of the tantalum triangle.

## 1. Introduction

Gas-phase transition-metal carbides have been the subject of much investigation for several decades.<sup>1–4</sup> This field of research has been reinvigorated with the development of the laser ablation source by Smalley and co-workers which has allowed the investigation of molecules containing refractory metals.<sup>5–7</sup> For example, the production and fragmentation of tantalum–carbide cluster ions was studied by McElvany and Cassady in 1990 following laser vaporization of a pressed Ta/C pellet (1:4 molar ratio) and ion injection into a Fourier transform ion cyclotron mass spectrometer.<sup>8</sup> With this technique McElvany and Cassady reported  $Ta_mC_n^+$  clusters with  $m = 1–11$  and  $n = 1–26$  but found that  $TaC_2^+$  and  $TaC_4^+$  clusters had an enhanced abundance. This is consistent with earlier Knudsen effusion mass spectrometric studies of other early transition metal carbides, which suggested the presence of strong metal–dicarbide ( $M-C_2$  and  $C_2-M-C_2$ ) bonds resulting from the pseudo-oxygen character of the  $C_2$  radical.<sup>1–4</sup> McElvany and Cassady also performed low-energy collision-induced dissociation experiments which predominantly showed the loss of neutral  $C_3$  and  $C_{10}$  groups. A subsequent study investigating the reaction of  $Ta_mC_n^+$  cluster ions with deuterium and various hydrocarbons concluded that the reactions are initiated on the metal center.<sup>9</sup>

A couple of years later, Castleman and co-workers discovered that various transition metals such as Ti, V, Zr, and Hf formed metal–carbide cluster ions of the form  $M_8C_{12}^+$  which were labeled metallocarbohedrenes or “Met-Cars”.<sup>10,11</sup> These clusters were formed following the reaction of gaseous metal and various hydrocarbons in a laser-induced plasma producing cationic clusters which were subsequently detected in a mass spectrometer. Peaks corresponding to eight metal atoms and 12 carbon atoms, hereafter denoted as (8,12), were found to be particularly stable, which was accounted for by a cagelike pentagonal dodecahedron structure. Other metals such as Cr, Fe, and Mo

were also found to preferentially form “Met-Cars”.<sup>12</sup> This work was quickly followed by studies that showed neutral “Met-Cars” of Ti, V, and Zr were also generated in a laser ablation source simultaneously with the cations. These neutrals were detected as the corresponding cations following laser ionization.<sup>12–14</sup>

Castleman and co-workers extended their studies and showed that niobium was another member of the “Met-Car” family and that niobium–carbide clusters were produced as both neutrals and cations.<sup>15</sup> However, it was shown that apart from the (8,12) stoichiometry, magic numbers also appeared at (4,4) and (14,13) corresponding to face-centered cubic (fcc) structures of dimension  $2 \times 2 \times 2$  and  $3 \times 3 \times 3$ , respectively. Castleman and co-workers then showed that by varying the conditions of the plasma it was possible to preferentially form either cubes or “Met-Cars”, thereby establishing that, apart from obvious thermodynamic considerations, kinetic factors are also involved in the formation of metal–carbon clusters. Subsequent work by Brock and Duncan<sup>16</sup> on neutral niobium–carbon clusters corroborated these findings and also determined approximate ionization potentials for  $Nb_8C_{12}$  and  $Nb_4C_4$ .

In contrast with vanadium and niobium, the next group V element, tantalum, has received scant attention. Castleman and co-workers showed that Ta predominantly formed metal–carbide clusters of the form (14,13), (18,18), (24,24), (32,32), (40,40), and (50,50),<sup>13</sup> which are stoichiometries consistent with face-centered cubic structures. Hackett and co-workers have also published mass spectra of tantalum–carbide clusters following the reaction of laser-ablated tantalum with propane and subsequent ionization with one (220 nm) or two (308 nm) photons.<sup>17</sup> However, these workers do not make detailed comment on the observed stoichiometries. These studies, including the earlier work of McElvany and Cassady,<sup>8,9</sup> represent the only experimental reports of tantalum–carbide clusters. Theoretical studies of TaC,  $TaC^+$ ,  $TaC_2^+$ , and  $TaC_n^+$  ( $n = 7–13$ ) have been reported by Balasubramanian and co-workers.<sup>18–20</sup> From their work,  $TaC_2^+$  was shown to adopt both a linear configuration of the form Ta–C–C and a “T-shaped” configuration with the

\* Corresponding author. Fax: +61 8 8303 4358. E-mail: gregory.metha@adelaide.edu.au.

former being slightly more stable. Various geometric isomers of  $\text{TaC}_n^+$  ( $n = 7\text{--}13$ ) were found to adopt either metallacycle, linear, bridged, atop, or metallocenic structures.

In this paper, we show experimental evidence that neutral tantalum–carbide clusters are formed which are smaller than those produced by Castleman and co-workers.<sup>13</sup> Furthermore, we have employed computational methods to calculate the lowest energy structures for the neutral clusters  $\text{Ta}_m\text{C}_n$  ( $m = 1\text{--}4$ ,  $n = 0\text{--}4$ ). Our work shows that the very small  $\text{Ta}_m\text{C}_n$  clusters adopt geometries that are subunits of the face-centered cubic structure.

## 2. Experimental and Computational Methods

**2.1. Experiment.** The tantalum–carbide clusters are formed in a laser ablation source coupled to a reflectron time-of-flight mass spectrometer. A detailed description is provided below since the experimental arrangements have not been described before. The ablation source is modeled on that used by Merer and co-workers<sup>21</sup> and the time-of-flight reflectron spectrometer is based on a design originally described by Johnson and co-workers.<sup>22</sup>

A gas mix consisting of 8% acetylene (BOC gases, 99%) seeded in 170 kPa helium (CIG gases, 99.98%) flows into the reaction region via a pulsed nozzle (General Valve, series 9, 500  $\mu\text{m}$  orifice) which is driven by a commercial nozzle driver (CPC, PND-1). A tantalum rod (Pure Tech, 99.5%), continually rotated and translated (Oriol, motor-mike 18014), is ablated with  $\sim 1$  mJ of the second harmonic from a pulsed Nd:YAG laser (Big Sky Laser, ULTRA-CFR). The resulting mixture is passed along a 5 mm long, 2 mm diameter reaction channel, or “condensation tube”, before being expanded into the first vacuum chamber. The clusters pass through a home-built 3 mm skimmer into the ionization region of a Wiley–McLaren time-of-flight mass spectrometer arranged collinear with the cluster beam. The neutral clusters are ionized with the output from a second Nd:YAG laser (Spectra-Physics GCR-170–10). Both the second (532 nm) and third (355 nm) harmonics were used to intersect the molecular beam perpendicularly within the extraction region. The ionizing radiation is focused with a 250 mm quartz planoconvex lens to a spot approximately 1 mm in diameter. Typical laser powers are around 1 mJ/pulse, which corresponds to power densities of  $\sim 130$  mJ/cm<sup>2</sup> or  $\sim 2 \times 10^7$  W/cm<sup>2</sup>. Resulting ions are then extracted into the second chamber containing an Einzel lens and a set of deflection plates before passing into the third vacuum chamber where they are reflected with a multistage reflectron onto an MSP ion detector (EI Mul, E033A).

The collinear arrangement of the cluster formation/time-of-flight instrument is important as it means that all masses arrive at the detector with equal efficiency; that is, there is no “mass window” effect, as is often observed in perpendicular time-of-flight instruments. The reflectron is also insensitive to mass, and we have conducted experiments to show that the cluster distribution before and after the reflectron is identical. Moreover, variations in ion deflection and focusing voltages and pulse delay times were found to have a negligible effect on the observed cluster distributions.

The output signal is amplified 10-fold with a home-built fast preamplifier before being displayed on a digital oscilloscope (LeCroy 9350AM). Each mass spectrum is averaged over 500 laser pulses, and the resulting data are downloaded to a computer. The timing for the experiment is provided with a digital delay generator (Griffith University, TARDIS II) which ensures pulse-to-pulse stability to within 1 ns. The laser power

is measured with a pyrometer (Scientech PHD25) used in statistics mode to calculate the pulse-to-pulse variation of the ionization laser power during the collection of each mass spectrum.

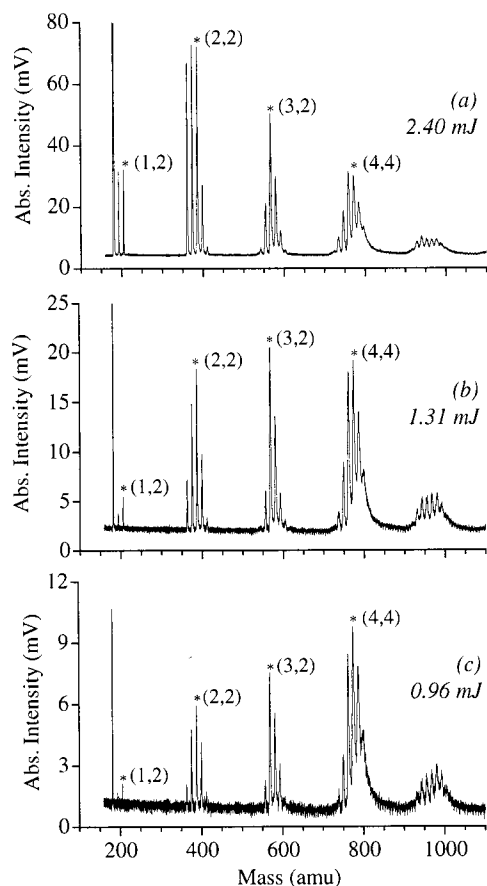
The first vacuum chamber is pumped by a cryogenically cooled pumping station (Varian VHS-6, Welch 1397) which maintains a working pressure of  $1.5 \times 10^{-5}$  Torr. The second and third vacuum chambers are similarly pumped (Varian M-6, Welch 1397) and maintain operational pressures of  $1 \times 10^{-6}$  and  $1 \times 10^{-7}$  Torr, respectively.

**2.2. Computation.** Geometry optimization and harmonic vibrational frequency calculations were performed using density functional theory in the Gaussian 94 suite of programs.<sup>23</sup> The calculations were performed with the B3P86 method using the LANL2DZ basis set. The LANL2DZ basis set employs the Dunning/Huzinaga double- $\zeta$  descriptor<sup>24</sup> for the carbon atoms and replaces the core electrons of tantalum atoms (up to 4f) with the effective core potentials of Hay and Wadt.<sup>25</sup> This method and basis set are the same as those used by Hackett and co-workers to calculate structures of various niobium clusters,  $\text{Nb}_3\text{O}$ ,  $\text{Nb}_3\text{C}_2$ , and  $\text{Nb}_3\text{N}_2$ .<sup>26–28</sup> Initially, all structures were performed without any geometry constraint. Many initial geometries were used leading to various local minima, usually separated by several electronvolts of energy. All minima were characterized with vibrational frequency calculations to determine whether each optimized structure was a true minimum and not a saddle point. The globally minimized structure for each stoichiometry was then examined to determine any symmetry properties and the calculations were again repeated within the highest symmetry point group. The symmetry-constrained energy was then compared to the unconstrained energy to ensure that there was no difference. Following this, harmonic vibrational frequencies were also recalculated within the point group to determine the frequency and symmetry of each normal mode of vibration. Calculations on clusters possessing an even and odd number of tantalum atoms were only performed with singlet and doublet multiplicity, respectively.

## 3. Results and Discussion

**3.1. Mass Spectra.** A typical mass spectrum is shown in Figure 1a using 2.40 mJ of 532 nm as the ionizing radiation. The mass spectrum shows five distinct groups of peaks corresponding to 1–5 tantalum atoms with the atomic peak,  $\text{Ta}^+$  ( $m/z = 181$ ), being the most intense (truncated in this spectrum). Within each group of peaks there are a series of peaks corresponding to different numbers of carbon atoms in the cluster. It is obvious that certain stoichiometries are favored and some of the more intense peaks are labeled ( $m,n$ ) where the two numbers indicate the number of tantalum ( $m$ ) and carbon ( $n$ ) atoms, respectively. The spectrum shows that the addition of successive tantalum atoms decreases the intensity of each group from  $\text{TaC}_n^+$  through to  $\text{Ta}_4\text{C}_n^+$ . Thereafter, a significant intensity decrease is observed for  $\text{Ta}_5\text{C}_n^+$ .

We cannot compare the spectrum in Figure 1a with that obtained by Castleman and co-workers since their published mass spectrum begins at 2000 amu and extends to over 10 000 amu.<sup>13</sup> Furthermore, no mention is made by these workers of intense peaks below 2000 amu. We have observed clusters containing up to six tantalum atoms and no more. There are intrinsic differences between our experiment and that of Castleman and co-workers. First, the power of our ablation laser is  $\sim 2$  mJ/pulse compared to 5–30 mJ/pulse, although both



**Figure 1.** Mass spectra of tantalum-carbide clusters,  $Ta_mC_n$ , following ionization with 532 nm at various laser powers: (a) 2.40; (b) 1.31; (c) 0.96 mJ. Note that the  $Ta^+$  peak is truncated in (a) and (b). Selected clusters are identified with an asterisk (\*) above them and are labeled  $(m,n)$  which corresponds to the number of tantalum and carbon atoms, respectively.

experiments use 532 nm as the ionizing wavelength. Second, and more importantly, Castleman and co-workers use a 0.5'' long "waiting room" tube and conical nozzle between the ablation region and the start of the supersonic expansion. This is in contrast with our relatively short 5 mm long "condensation tube" which terminates directly at the expansion region. The former arrangement allows more collisions thereby allowing larger clusters to form. It is well-known that longer "condensation tubes" are used to form larger metal clusters.<sup>29,30</sup>

It is also difficult to compare our spectrum to that of McElvany et al. who generated tantalum-carbide cluster ions by ablating a pressed pellet of 1:4 Ta/C at 532 nm (5–30 mJ/pulse) and injected them into an FT-ICR-MS.<sup>8,9</sup> It should be reiterated that the differences between their experiment and ours are major; they observe ions directly formed from the ablation process of a mixed tantalum-carbon pellet which are observed under thermalized conditions, whereas we observe neutral clusters formed by the reaction of acetylene and ablated tantalum which are cooled in a supersonic expansion and subsequently laser ionized. The mass spectrum of McElvany et al. shows  $Ta_mC_n^+$  clusters ( $m = 1-4$  and  $n = 1-16$ ) with the  $Ta_2C_3^+$  peak being the most intense. The intensity of the peaks falls off between  $Ta_2C_n^+$  and  $Ta_4C_n^+$ , and many more carbons are attached to each tantalum atom than we observe. Their published spectrum does not extend past  $Ta_4C_n^+$  and so it not possible to determine whether a large intensity decrease is observed upon addition of a fifth tantalum atom.

On the basis of the observed distributions, it is possible to speculate on the chemistry processes occurring in the ablation/

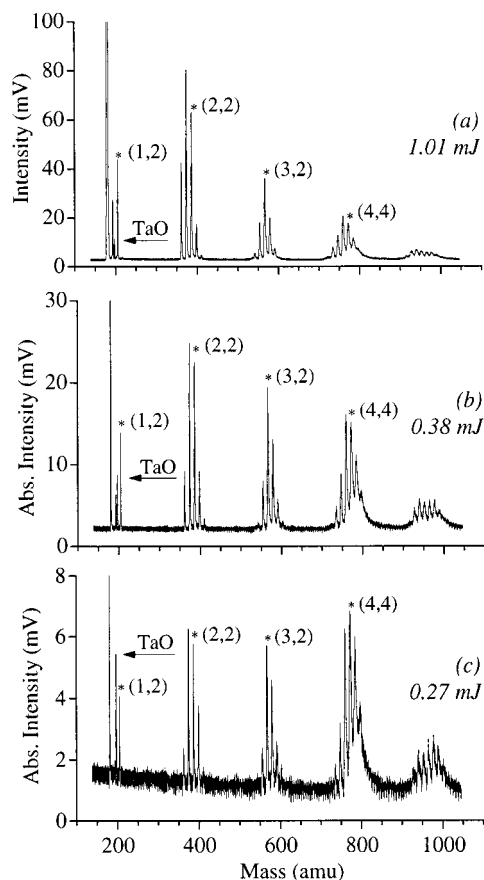
reaction source. The fact that the most intense clusters observed within each group have a relative Ta to C ratio of 1:1 would suggest that the building blocks for cluster formation are TaC units. We have found the cluster distribution to be invariant as the concentration of  $C_2H_2$  reactant gas is increased from 8% to 24%, which implies that larger hydrocarbon concentrations do not induce the formation of  $TaC_2$  building block units. Furthermore, the reaction of 5%  $CH_4$ , instead of  $C_2H_2$ , was found to produce an identical cluster distribution which also suggests that TaC, and not  $TaC_2$ , is the cluster building block unit.

Since the energy of the ionizing radiation in our experiments is so low (i.e., 532 and 355 nm, or 2.33 and 3.49 eV, respectively), it is assumed that multiple photon absorption is required for ionization to be achieved. The ionization potential (IP) of  $Nb_3C_2$  is known from pulsed field ionization-zero electron kinetic energy spectroscopy to be 5.038 eV, and the IP of  $Nb_4C_4$  and  $Nb_5C_2$  is known from photoionization efficiency spectroscopy to be 4.43 and 4.59 eV, respectively.<sup>27</sup> Furthermore, the ionization potentials of bare tantalum clusters are also known to be in the same energy regime;  $Ta_2$  is 5.98–6.42 eV, and  $Ta_3$  is 5.58 eV.<sup>31</sup> Therefore, high photon fluences are required to achieve nonresonant ionization. This is consistent with the fact that we are using laser powers of  $> 1$  mJ, equating to a fluence of  $> 130$  mJ/cm<sup>2</sup> upon focusing, in comparison with laser fluences of 5–400  $\mu$ J/cm<sup>2</sup> (unfocused) for the  $Nb_4C_4$  study and  $\sim 300$   $\mu$ J/cm<sup>2</sup> (unfocused) for the  $Nb_3C_2$  study.

The mass spectra shown in parts b and c of Figure 1 are recorded under identical conditions to Figure 1a except that the ionization laser is operated at lower power, the laser powers being 1.31 and 0.96 mJ, respectively. As expected, the absolute intensity of each cluster peak decreases with decreasing laser power. However, the relative intensity of each cluster peak also changes with the ionization power. These two observations will be discussed later.

Figure 2a shows a mass spectrum collected using 1.01 mJ of 355 nm as the ionizing radiation. The observed cluster distribution is very similar to that shown in Figure 1a (532 nm), with one exception. This exception is the appearance of a peak corresponding to  $TaO^+$  using 355 nm ionization, although it is less than half the intensity of the  $TaC^+$  peak. It is quite common for oxides of transition metals to appear in mass spectra since the oxides are usually present as an impurity on the coating of the metal rod. Indeed, we have observed oxides of titanium and tungsten under similar conditions, and the fact that the overall intensity of  $TaO^+$  is quite low, in comparison with the tantalum-carbide peaks, is probably due to the fact that there is very little oxide present which limits the production of neutral TaO. However, it is unusual that  $TaO^+$  appears at 355 nm and not at 532 nm and a possible explanation is as follows. The ionization potential of TaO is known to be  $8.61 \pm 0.02$  eV<sup>32</sup> which would require  $4 \times 532$  nm photons (9.32 eV) or  $3 \times 355$  nm photons (10.48 eV). Furthermore, TaO is known to have a  $X^2\Delta_{3/2}$  ground state and many excited states have been identified by both gas-phase emission<sup>33–36</sup> and matrix absorption<sup>37</sup> studies in the visible and near-ultraviolet. The origin of the  $P^2\Delta_{3/2} \rightarrow X^2\Delta_{3/2}$  transition is known to be at 374.7 nm in the gas phase. Transitions to one and two quanta of vibration in the excited state ( $\sim 902$  cm<sup>-1</sup>) give rise to transitions around 362.2 and 350.7 nm, respectively. Therefore, 355 nm falls between one and two quanta of the vibration built upon the electronic origin. We postulate that the near-resonant step of the first photon at 355 nm enhances the probability of  $TaO^+$  ions forming, whereas there are no corresponding vibronic states





**Figure 2.** Mass spectra of tantalum–carbide clusters,  $Ta_mC_n$ , following ionization with 355 nm at various laser powers: (a) 1.01; (b) 0.38; (c) 0.27 mJ. Note that the  $Ta^+$  peak is truncated in all three spectra. Selected clusters are identified with an asterisk (\*) above them and are labeled  $(m,n)$  which corresponds to the number of tantalum and carbon atoms, respectively. Also note the presence of tantalum oxide which is indicated with a horizontal arrow at the same height as the  $TaO^+$  peak.

near 532 nm. We intend to confirm or deny the above postulate by recording a one-color resonance-enhanced multiphoton ionization spectrum of  $TaO$  around 355 nm employing a 1+2 ionization scheme.

The mass spectra shown in parts b and c of Figure 2 are recorded using lower ionization powers at 355 nm than used for Figure 2a. As we found for the mass spectra recorded at 532 nm, both the *absolute* and *relative* intensity of each cluster peak changes with decreasing 355 nm laser power. This is similarly true for the  $TaO^+$  peak. These intensity changes will now be addressed.

It is tempting to attribute the ion intensities in the mass spectra to nascent distributions of neutral clusters formed within the ablation source. However, the intensity of each ion in the mass spectra is a function of several factors: the nascent neutral cluster distribution, the ionization potential of each cluster, the ionization cross section of each cluster, and finally, the propensity for photoinduced cluster fragmentation, especially at higher laser fluences.

For a nonresonant multiphoton absorption resulting in ionization, the relationship between ion signal and laser power can usually be described as

$$\text{ion signal} \propto (\text{laser power})^N$$

where  $N$  is the number of photons required to achieve ionization and is strictly an integer.<sup>29</sup> There are several examples of power dependence experiments in the literature performed on pure

metal clusters such as  $Fe_n$ <sup>29</sup> and  $Ni_n$ <sup>30</sup> by Kaldor and co-workers. Their experiments were performed using wavelengths of 193 nm ( $\sim 6.4$  eV), and the power dependence was found to be either linear or quadratic with respect to laser power, indicating that one or two photons were required for ionization, respectively. More recent work by Brock and Duncan on near-threshold photoionization of several “Met-Cars” and  $Nb_4C_4$ <sup>16</sup> revealed more complex behavior. At 215 nm, the  $V_8C_{12}$  and  $Zr_8C_{12}$  clusters show a dependence of  $N = 2.26$  and 2.47, respectively, and the  $Nb_4C_4$  cluster shows a dependence of 2.39. Brock and Duncan interpreted these results by arguing that at least two photons were required for ionization. These results indicate that the simple formula given above is not generally applicable even when only two photons are required for ionization. At the wavelengths used in our studies (532 and 355 nm), three or four photons are required for ionization of  $Ta_mC_n$  species and we have found that the power dependence method does not correctly determine the number of photons required for ionization. This work is currently being prepared for publication.<sup>38</sup> To obtain accurate ionization potentials of the  $Ta_mC_n$  clusters, photoionization efficiency experiments are currently being undertaken in our laboratory.

Without knowledge of the ionization potential, we are still able to offer some preliminary comments pertaining to the potentially competing processes at play. At lower laser powers (parts b and c of Figure 1 and parts b and c of Figure 2), both the absolute and relative intensity distributions are observed to change, suggesting that both multiple photon ionization and fragmentation may be occurring. However, at 532 nm, for laser powers of  $\sim 2$  mJ/pulse and greater, the ion distributions do not change and appear as shown in Figure 1a. This is similarly true at 355 nm for laser powers of  $\sim 1$  mJ/pulse and greater (Figure 2a). This indicates that all neutral species in the laser interaction region have been ionized. Furthermore, any fragmentation that *may* have been occurring at low laser fluences has also been saturated. Our continuing studies at lower photon wavelengths (i.e., in the one-photon ionization regime) will eliminate fragmentation due to multiple photon absorption. This will allow us to determine the nascent neutral cluster distribution generated in our source.

One final comment about the mass spectra relates to the observed asymmetry of the  $Ta_4C_n^+$  peaks and to a lesser extent the  $Ta_5C_n^+$  peaks. This asymmetry has been observed in niobium clusters following multiphoton ionization and was found to be negligible following ionization with a single photon. Two different explanations have been proposed. The first possibility is that the tailing of these peaks is due to unimolecular decay of higher mass cluster ions in the acceleration region of the mass spectrometer.<sup>39</sup> This seems a likely explanation given that we suspect a certain amount of fragmentation to be occurring. The other possibility is that of delayed ionization which is analogous to the bulk property of thermionic emission.<sup>17</sup> Since the asymmetry effect is small in our tantalum–carbide work, and we were able to assign the individual mass peaks of interest, no further investigation of the effect was made.

For the reasons mentioned above, it is impossible to extract quantitative information about the relative stability of tantalum–carbide clusters from the mass spectra. However, it is possible to qualitatively deduce that some clusters are relatively more stable than others. Each of the six mass spectra in Figures 1 and 2 shows a significant intensity drop from  $Ta_4C_n^+$  to  $Ta_5C_n^+$ . This is suggestive of an enhanced stability for neutral  $Ta_4C_n$  clusters. Castleman and co-workers have postulated that larger tantalum–carbide clusters form face-centered cubic (fcc) struc-

tures,<sup>13</sup> for example, their (14,13) mass peak corresponds to a  $3 \times 3 \times 3$  fcc lattice. Therefore, we can infer that  $\text{Ta}_4\text{C}_4$  is also a cubic structure corresponding to a  $2 \times 2 \times 2$  fcc lattice. To explore this, we have undertaken theoretical calculations using density functional theory to characterize the structures of neutral tantalum–carbide clusters. These results are presented and discussed in the following section.

**3.2. DFT Calculations.** We have explored the structures of various neutral tantalum–carbide clusters using density functional theory. The use of modest levels of theory and basis sets has allowed us to compute minimized geometries and harmonic frequencies for a large range of these clusters. Following is a discussion on each of the tantalum–carbide clusters  $\text{Ta}_m\text{C}_n$  for  $m = 1-4$  and  $n = 0-4$ . Table 1 shows the calculated geometry for the global minimum for each cluster, and Table 2 shows the absolute energy, point group symmetry, and harmonic vibrational frequencies for each cluster.

**$\text{TaC}_n$  Clusters.** Tantalum carbide,  $\text{TaC}$ , is calculated to have a bond length of 1.76 Å and a vibrational frequency of 977  $\text{cm}^{-1}$ . Majumdar and Balasubramanian have recently performed calculations on  $\text{TaC}$  and  $\text{TaC}^+$  utilizing relativistic complete active space self-consistent field (CASSCF) and multireference configuration interaction (MRCI).<sup>18</sup> They found  $\text{TaC}$  to have a  $^2\Sigma^+$  ground state with a bond length of 1.791 Å and a frequency of 748  $\text{cm}^{-1}$ . The two bond lengths are in reasonable agreement, particularly considering the vastly different computational methods used; however, the two frequencies differ substantially. It is interesting to note that Majumdar and Balasubramanian's calculations on  $\text{TaC}^+$  indicate a  $^1\Sigma^+$  ground state with a bond length of 1.731 Å and a frequency of 1307  $\text{cm}^{-1}$  and a nearby  $^3\Sigma^+$  state only 0.12 eV higher in energy.

Tantalum dicarbide was found to adopt a “T-shaped” geometry of  $C_{2v}$  symmetry with a Ta–C bond length of 1.91 Å, a C–C bond length of 1.43 Å, and a C–Ta–C angle of 44°. Although the geometry optimization was successful, we had difficulty determining the vibrational frequencies and so they are not listed in Table 2. Roszak and Balasubramanian have performed CASSCF and MRCI calculations on  $\text{TaC}_2^+$  and found two near degenerate minima: a “T-shaped” isomer of  $C_{2v}$  symmetry ( $^3A_2$  state) and an asymmetric linear isomer, Ta–C–C, of  $C_{\infty v}$  symmetry ( $^3\Delta$  state).<sup>19</sup> It is possible that difficulties in calculating vibrational frequencies for  $\text{TaC}_2$  using the B3P86 theoretical approach are attributable to a mixing of the bent and linear geometric descriptions within the DFT calculations.

Although our attempts to find a minimum corresponding to the linear isomer resulted in a single-point calculation of lower energy than the “T-shaped” isomer, all attempts to calculate an optimized geometry were unsuccessful. Further work at higher levels of theory is needed to better understand the  $\text{TaC}_2$  system. If the  $\text{TaC}_2$  neutral can be shown by theory to have both electronically stable bent and linear isomers of near degeneracy, as has the cation, it is likely that both isomers will be present in the supersonic molecular beam and it should be possible to devise spectroscopic experiments to interrogate this system.

The mass spectra in Figures 1 and 2 show only the faintest hint of tantalum tricarbide,  $\text{TaC}_3$ , and no evidence appears for tantalum tetracarbide,  $\text{TaC}_4$ . However, the calculated structures can help to determine whether an increasing number of carbons reveals a structural pattern.  $\text{TaC}_3$  was calculated to have  $C_{2v}$  symmetry which can be thought of as a slightly bent  $C_3$  unit attached to the tantalum atom to form an  $\eta^3$ -bond. The two distinct Ta–C bond lengths are 1.96 and 2.03 Å, slightly longer than that calculated for  $\text{TaC}_2$ . The C–C bond lengths are both 1.37 Å, slightly shorter than in  $\text{TaC}_2$ .

Similarly,  $\text{TaC}_4$  was also calculated to have  $C_{2v}$  symmetry and continues the motif of carbon atoms encircling the tantalum atom to form an  $\eta^4$ -bond. The two distinct Ta–C bond lengths are now 2.02 and 2.11 Å, and both the C–C bond lengths are about 1.38 Å. It is presumed that the addition of further carbon atoms would continue the trend of bonding around the tantalum atom. Calculations of various isomers of  $\text{TaC}_n^+$  ( $n = 7-13$ ) have been performed by Roszak and Balasubramanian using self-consistent field Hartree–Fock and density functional methods.<sup>20</sup> They found that the  $\text{TaC}_7^+$  structure is an open chain and that  $\text{TaC}_8^+$  is cyclic. It is not until nine or more carbon atoms are added that metallocenic structures, where the carbon atoms completely encircle a single tantalum atom, are formed. Consistent with the notion of a preference for metallocene formation, we could not find stable minima for either the C–C–Ta–C–C linear isomer or the  $C_2$ –Ta– $C_2$  “double T-shaped” isomer.


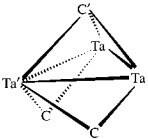
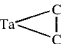
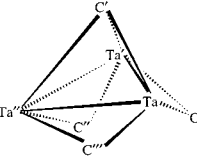

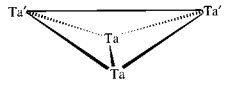

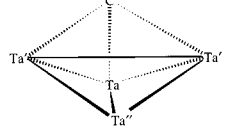
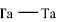
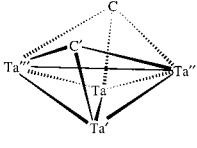
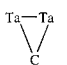
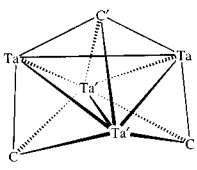
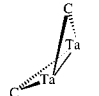
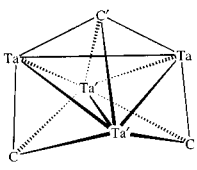
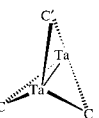
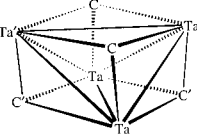
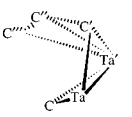
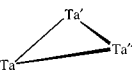
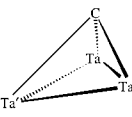
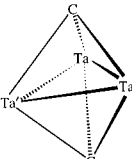
**$\text{Ta}_2\text{C}_n$  Clusters.** Very little is known about the tantalum dimer,  $\text{Ta}_2$ , which is quite prevalent in the mass spectra of Figures 1 and 2. Our calculations on the lowest singlet state predict a bond length of 2.15 Å and a vibrational frequency of 354  $\text{cm}^{-1}$ . From the few experimental studies reported on  $\text{Ta}_2$ , the ionization potential is known to lie between 5.98 and 6.42 eV<sup>31</sup> and the bond energy is known to be between 4.96 and 5.40 eV.<sup>40</sup> Furthermore, Simard et al.<sup>40</sup> have recorded laser-induced fluorescence spectra in the 535–680 nm range which show that the ground state has a frequency of about 280  $\text{cm}^{-1}$ , in reasonable agreement with our calculation. Collection and analysis of higher resolution spectra are currently underway by the same workers.

The lowest energy structure of  $\text{Ta}_2\text{C}$  has a bent geometry with  $C_{2v}$  symmetry. The Ta–Ta bond length has increased slightly to 2.30 Å from  $\text{Ta}_2$ , and the Ta–C bond length is 1.96 Å. The addition of a second carbon atom produces a “butterfly” geometry of  $C_{2v}$  symmetry in which the Ta–Ta bond length has increased to 2.52 Å while the Ta–C bond lengths have reduced slightly to 1.92 Å. The “butterfly” geometry is an example of an *arachno* structure which is well-known in condensed phase organometallic cluster molecules containing four metal atoms.<sup>41</sup> *Arachno* structures result when one of the metal–metal bonds of a tetrahedron is broken to form the “hinge” and two “wingtips” of the *arachno*-butterfly motif.

$\text{Ta}_2\text{C}_3$  is shown to possess  $C_{2v}$  symmetry, only slightly distorted from an idealized  $D_{3h}$  structure in which three carbon atoms are bonded evenly around the Ta–Ta “hinge”. All Ta–C bond lengths are identical, and the higher symmetry is only lost because the three dihedral angles are not exactly 120.0°. Unfortunately, we could not achieve wave function convergence at  $D_{3h}$  symmetry, although various convergence methods were used with the B3P86/LANL2DZ method. Despite this, we believe that the minimum structure should be of  $D_{3h}$  symmetry. Calculations at higher levels of theory may be necessary to address this issue. In comparison with  $\text{Ta}_2\text{C}_2$ , the Ta–C bond lengths have increased slightly to 1.97 Å.

Following the pattern thus far, the addition of a fourth carbon atom would also be expected to bond around the Ta–Ta “hinge”. However, the  $\text{Ta}_2\text{C}_4$  cluster shows a departure from this expectation and the lowest energy geometry is as shown in Table 1. The structure can be thought of as a combination of the  $\text{Ta}_2\text{C}_2$  “butterfly” moiety and the  $\eta^3$ -bonding moiety shown for  $\text{TaC}_3$ . We also calculated two other minima, including the isomer with all four carbon atoms bonded around the Ta–Ta “hinge”, but these were found to be at least 1 eV higher in energy.

TABLE 1: Global Minimum Geometry for Each Cluster Calculated Using the B3P86/LANL2DZ Method<sup>a</sup>

Cluster (Symmetry)	Structure	Bond Lengths (Å)	Bond Angles and Dihedrals (Degrees)	Cluster (Symmetry)	Structure	Bond Lengths (Å)	Bond Angles and Dihedrals (Degrees)
TaC $2\Sigma^+ (C_{\infty})$		Ta-C = 1.76		Ta <sub>3</sub> C <sub>3</sub> $2A' (C_3)$		Ta-Ta = 2.70 Ta-Ta' = 2.80 Ta-C = 1.89 Ta'-C = 1.96 Ta'-C = 2.04 Ta'-C' = 2.04	C-Ta'-Ta = 42.3 C-Ta-Ta' = 44.4 C'-Ta'-Ta = 46.7 C'-Ta-Ta' = 46.7 Ta-C-Ta' = 83.0 C'-Ta-Ta'-C = 161.1 C-Ta-Ta'-C = 140.2
TaC <sub>2</sub> $2B_2 (C_{2v})$		Ta-C = 1.91 C-C = 1.43	Ta-C-C = 68.1 C-Ta-C = 43.8	Ta <sub>3</sub> C <sub>4</sub> $2A (C_1)$		Ta-Ta' = 2.82 Ta-Ta'' = 2.87 Ta'-Ta'' = 2.89 Ta-C = 1.92 Ta-C' = 2.05 Ta-C''' = 1.99 Ta'-C = 1.93 Ta'-C' = 2.05 Ta'-C'' = 1.99 Ta''-C' = 2.03 Ta''-C'' = 1.95 Ta''-C''' = 1.94	C'-Ta-Ta' = 46.5 Ta-C'-Ta' = 87.1 C'-Ta'-Ta'' = 44.6 C'-Ta''-Ta' = 45.1 C'-Ta-Ta'' = 45.4 C'-Ta-Ta'' = 44.9 Ta-Ta'-Ta'' = 60.5 Ta-Ta''-Ta' = 58.6 Ta-Ta'-C = 43.1 Ta-Ta'-C' = 42.9 Ta-Ta'-C'' = 43.4 Ta-Ta'-C''' = 42.3 Ta-Ta''-C''' = 43.5 Ta-Ta''-C'''' = 42.2 C'-Ta''-Ta'-C'' = -174.7 C'-Ta-Ta'-C = -161.9 C'-Ta-Ta'-C''' = -172.5
TaC <sub>3</sub> $2A_1 (C_{2v})$		Ta-C = 1.96 Ta-C' = 2.03 C-C' = 1.37	Ta-C-C' = 72.7 Ta-C'-C = 67.0 C-Ta-C' = 40.3	Ta <sub>4</sub> $1A_1 (C_{2v})$		Ta-Ta = 2.53 Ta-Ta' = 2.48 Ta'-Ta' = 3.28	Ta-Ta'-Ta = 61.3 Ta-Ta-Ta' = 100.4 Ta-Ta'-Ta-Ta' = -85.5
TaC <sub>4</sub> $2A_1 (C_{2v})$		Ta-C = 2.11 Ta-C' = 2.02 C-C' = 1.38 C'-C' = 1.39	C-Ta-C' = 38.8 C'-Ta-C' = 40.2	Ta <sub>4</sub> C $1A' (C_2)$		Ta-Ta' = 2.54 Ta-Ta'' = 2.58 Ta'-Ta' = 2.93 Ta'-Ta'' = 2.53 Ta-C = 2.45 Ta'-C = 1.96	Ta-Ta'-Ta = 59.2 Ta-Ta-Ta' = 59.6 Ta-Ta-Ta' = 70.4 Ta-Ta-Ta'-C = 46.3 Ta'-C-Ta'' = 69.0 Ta'-C-Ta' = 96.5 C-Ta-Ta-Ta'' = -167.6
Ta <sub>2</sub> $1\Sigma_g^+ (D_{\infty h})$		Ta-Ta = 2.15		Ta <sub>4</sub> C <sub>2</sub> $1A (C_1)$		Ta-Ta' = 2.59 Ta-Ta'' = 2.58 Ta-Ta''' = 2.53 Ta'-Ta'' = 2.89 Ta'-Ta''' = 2.59 Ta'-Ta'''' = 2.86 Ta-C = 2.37 Ta'-C = 1.96 Ta'-C' = 1.96 Ta'-C'' = 1.98 Ta''-C' = 1.97 Ta''-C'' = 2.31	C'-Ta-Ta'-Ta' = 46.7 Ta-Ta'-C'-Ta' = 74.0 C'-Ta-Ta'-Ta' = 42.5 Ta'-C'-Ta' = 94.4 Ta'-C'-Ta'' = 83.3 C'-Ta-Ta'' = 53.3 Ta'-C-Ta'' = 93.3 C-Ta-Ta'' = 43.5 C-Ta-Ta'' = 47.3 Ta-C-Ta'' = 70.7 C-Ta-Ta'' = 46.5 Ta-C-Ta'' = 72.5 C-Ta-Ta'-C' = -15.3 C-Ta-Ta'-C'' = -152.6 Ta-Ta-Ta'-Ta'' = 76.4 Ta-Ta-Ta''-Ta' = -70.7
Ta <sub>2</sub> C $1A_1 (C_{2v})$		Ta-Ta = 2.30 Ta-C = 1.96	Ta-Ta-C = 54.1 Ta-C-Ta = 71.7	Ta <sub>3</sub> C <sub>2</sub> $1A (C_1)$		Ta-Ta = 3.75 Ta-Ta' = 2.65 Ta'-Ta' = 2.59 Ta-C = 1.98 Ta-C' = 1.97 Ta'-C = 2.10 Ta'-C' = 2.31	Ta-Ta'-Ta = 59.2 Ta-Ta-Ta' = 59.6 Ta-Ta-Ta' = 70.4 Ta-Ta'-C = 46.3 Ta'-C-Ta'' = 69.0 Ta'-C-Ta' = 96.5 C-Ta-Ta-Ta'' = -167.6
Ta <sub>2</sub> C <sub>2</sub> $1A_1 (C_{2v})$		Ta-Ta = 2.52 Ta-C = 1.92	C-Ta-Ta = 49.1 Ta-C-Ta = 81.1 C-Ta-Ta-C = 140.1	Ta <sub>3</sub> C <sub>3</sub> $1A_1 (C_{2v})$		Ta-Ta = 3.75 Ta-Ta' = 2.65 Ta'-Ta' = 2.59 Ta-C = 1.98 Ta-C' = 1.97 Ta'-C = 2.10 Ta'-C' = 2.31	Ta-Ta'-Ta = 59.2 Ta-Ta-Ta' = 59.6 Ta-Ta-Ta' = 70.4 Ta-Ta'-C = 46.3 Ta'-C-Ta'' = 69.0 Ta'-C-Ta' = 96.5 C-Ta-Ta-Ta'' = -167.6
Ta <sub>2</sub> C <sub>3</sub> $1A_1 (C_{2v})$		Ta-Ta = 2.52 Ta-C = 1.97 Ta-C' = 1.97	C-Ta-Ta = 50.1 C'-Ta-Ta-C = 120.0 C-Ta-Ta-C = 119.5	Ta <sub>3</sub> C <sub>4</sub> $1A_1 (C_{2v})$		Ta-Ta = 2.45 Ta-Ta' = 2.93 Ta'-Ta' = 2.87 Ta-C = 2.07 Ta-C' = 2.14 Ta'-C = 2.02 Ta'-C' = 1.94	Ta'-C'-Ta' = 69.8 Ta-C-Ta' = 90.7 Ta'-C-Ta = 91.3 Ta'-C'-Ta = 91.4 C'-Ta'-C = 84.3 C'-Ta'-Ta-C = -166.8 C'-Ta-Ta'-C' = 159.1 C-Ta-Ta-C = -166.3
Ta <sub>2</sub> C <sub>4</sub> $1A (C_1)$		Ta-Ta = 2.56 Ta-C = 1.93 Ta'-C = 1.92 Ta-C' = 1.95 Ta'-C' = 2.23 Ta'-C'' = 2.17 Ta'-C''' = 2.16 C'-C'' = 1.40 C''-C''' = 1.31	C-Ta'-Ta = 48.1 Ta-Ta'-C' = 47.1 C'-Ta'-C'' = 36.1 C''-Ta'-C''' = 35.1 C-Ta-Ta'-C' = 131.1 Ta-Ta'-C'-Ta'' = 152.1 C'-Ta'-C''-C''' = 176.1				
Ta <sub>3</sub> $2A'' (C_2)$		Ta-Ta' = 2.52 Ta'-Ta'' = 2.35 Ta''-Ta = 2.46	Ta-Ta'-Ta'' = 60.6 Ta'-Ta''-Ta = 63.1				
Ta <sub>3</sub> C $2A' (C_2)$		Ta-Ta = 2.61 Ta-Ta' = 2.44 Ta-C = 1.97 Ta'-C = 2.46	Ta-C-Ta = 83.4 C-Ta-Ta' = 65.8 C-Ta-Ta' = 67.0 Ta-Ta'-Ta = 64.7 C-Ta-Ta-Ta' = 86.8 Ta'-Ta-C-Ta = 66.3				
Ta <sub>3</sub> C <sub>2</sub> $2B_2 (C_{2v})$		Ta-Ta = 2.62 Ta-Ta' = 2.50 Ta-C = 2.07 Ta'-C = 2.06	Ta-C-Ta = 78.5 C-Ta-Ta' = 52.5 C-Ta-Ta' = 52.8 C-Ta-Ta-C = 130.1 C-Ta-Ta-C = 124.6				

<sup>a</sup> For each cluster, the calculated point group is listed along with all bond lengths, bond angles, and dihedral angles.

**Ta<sub>3</sub>C<sub>n</sub> Clusters.** The tantalum trimer, Ta<sub>3</sub>, has little intensity in the mass spectra and there are no known theoretical or experimental data. The lowest energy structure was found to be an irregular triangle with Ta–Ta bond lengths of 2.35, 2.46, and 2.52 Å, and attempts to constrain this molecule to higher than C<sub>s</sub> symmetry were unsuccessful. The irregular geometry can be rationalized by the fact that, under D<sub>3h</sub> symmetry, the unpaired electron would reside in a degenerate orbital thus leading to Jahn–Teller distortion which lowers the symmetry of the molecule.

In Ta<sub>3</sub>C, the lowest energy structure has the three tantalum atoms arranged in an isosceles triangle with the carbon atom

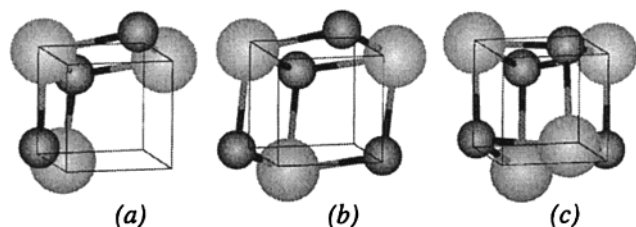
sitting above the triangle, out of the plane. However, the carbon atom is more closely bonded to two of the tantalum atoms (1.97 Å cf. 2.46 Å) to produce a structure of C<sub>s</sub> symmetry. A planar structure where the carbon atom is only bonded to two tantalum atoms was found to be 1.6 eV higher in energy.

It is expected that a second carbon atom would bond to the other side of the tantalum triangle, and this is indeed what is calculated for Ta<sub>3</sub>C<sub>2</sub>. However, there are two isomers found in which the two carbon atoms are either equally bonded to all three tantalum atoms, or where the two carbon atoms are closer to two of the tantalum atoms, the former being 0.3 eV lower in energy. We have already mentioned that an analogue of this



**TABLE 2: Absolute Energy, Point Group, and Harmonic Vibrational Frequencies Calculated for Each Cluster Using the B3P86/LANL2DZ Method**

cluster	absolute energy (H)	symmetry	vibrational frequencies (cm <sup>-1</sup> )
TaC	-96.0529105	$C_{\infty v}$	976.9 ( $\sigma^+$ )
TaC <sub>2</sub>	-134.2066425	$C_{2v}$	see text for details
TaC <sub>3</sub>	-172.4422376	$C_{2v}$	506.4 ( $b_2$ ), 581.9 ( $b_1$ ), 644.9 ( $a_1$ ), 847.4 ( $a_1$ ), 1214.7 ( $a_1$ ), 1424.9 ( $b_2$ )
TaC <sub>4</sub>	-210.6035806	$C_{2v}$	184.3 ( $b_1$ ), 327.6 ( $b_2$ ), 438.6 ( $a_1$ ), 535.6 ( $a_2$ ), 581.0 ( $b_2$ ), 645.7 ( $a_1$ ), 1007.5 ( $a_1$ ), 1303.4 ( $b_2$ ), 1590.0 ( $a_1$ )
Ta <sub>2</sub>	-115.9459500	$D_{\infty h}$	354.1 ( $\sigma_g^+$ )
Ta <sub>2</sub> C	-154.1708974	$C_{2v}$	285.1 ( $a_1$ ), 559.4 ( $b_2$ ), 803.4 ( $a_1$ )
Ta <sub>2</sub> C <sub>2</sub>	-192.4086670	$C_{2v}$	188.8 ( $a_1$ ), 392.2 ( $a_1$ ), 594.5 ( $a_2$ ), 799.0 ( $b_1$ ), 805.0 ( $b_2$ ), 889.3 ( $a_1$ )
Ta <sub>2</sub> C <sub>3</sub>	-230.5963109	$C_{2v}$	279.1 ( $a_1$ ), 290.7 ( $a_1$ ), 296.2 ( $b_1$ ), 561.6 ( $a_2$ ), 563.2 ( $b_2$ ), 734.8 ( $b_1$ ), 735.7 ( $a_1$ ), 740.9 ( $b_2$ ), 843.0 ( $a_1$ )
Ta <sub>2</sub> C <sub>4</sub>	-268.7491621	$C_1$	175.6, 191.9, 255.2, 308.7, 403.6, 496.4, 622.7, 650.5, 709.7, 833.3, 1204.7, 1678.0
Ta <sub>3</sub>	-174.0538892	$C_s$	104.5 ( $a'$ ), 180.5 ( $a'$ ), 272.5 ( $a'$ )
Ta <sub>3</sub> C	-212.2776256	$C_s$	125.1 ( $a''$ ), 178.3 ( $a'$ ), 247.4 ( $a'$ ), 250.6 ( $a'$ ), 572.6 ( $a''$ ), 749.5 ( $a'$ )
Ta <sub>3</sub> C <sub>2</sub>	-250.5174689	$C_{2v}$	52.2 ( $b_2$ ), 185.1 ( $a_1$ ), 234.6 ( $b_1$ ), 268.3 ( $a_2$ ), 282.8 ( $a_1$ ), 516.4 ( $a_1$ ), 537.6 ( $b_2$ ), 694.2 ( $b_1$ ), 812.1 ( $a_1$ )
Ta <sub>3</sub> C <sub>3</sub>	-288.7311503	$C_s$	77.9 ( $a''$ ), 162.7 ( $a'$ ), 189.7 ( $a''$ ), 241.9 ( $a'$ ), 325.0 ( $a'$ ), 481.0 ( $a''$ ), 550.2 ( $a'$ ), 672.4 ( $a'$ ), 693.7 ( $a''$ ), 802.2 ( $a'$ ), 840.8 ( $a''$ ), 868.9 ( $a'$ )
Ta <sub>3</sub> C <sub>4</sub>	-326.9310387	$C_1$	66.6, 207.5, 221.4, 247.8, 262.6, 344.8, 535.1, 596.0, 631.5, 649.9, 666.1, 746.4, 800.2, 816.2, 828.1
Ta <sub>4</sub>	-232.1618411	$C_{2v}$	78.1 ( $a_1$ ), 84.0 ( $a_2$ ), 176.3 ( $a_1$ ), 195.5 ( $b_2$ ), 202.4 ( $b_1$ ), 281.5 ( $a_1$ )
Ta <sub>4</sub> C	-270.4312683	$C_s$	129.9 ( $a'$ ), 145.3 ( $a''$ ), 179.2 ( $a'$ ), 185.8 ( $a''$ ), 208.3 ( $a'$ ), 267.3 ( $a'$ ), 280.9 ( $a'$ ), 700.4 ( $a''$ ), 735.3 ( $a'$ )
Ta <sub>4</sub> C <sub>2</sub>	-308.6477467	$C_1$	103.7, 126.9, 151.7, 163.9, 203.7, 247.8, 264.2, 371.8, 631.3, 705.2, 729.3, 750.1
Ta <sub>4</sub> C <sub>3</sub>	-346.8455655	$C_{2v}$	113.3 ( $a_2$ ), 127.9 ( $b_1$ ), 134.6 ( $a_1$ ), 168.8 ( $b_2$ ), 204.5 ( $a_1$ ), 259.5 ( $a_1$ ), 339.2 ( $b_1$ ), 422.1 ( $a_2$ ), 445.6 ( $b_1$ ), 448.4 ( $b_2$ ), 539.3 ( $a_1$ ), 618.2 ( $a_1$ ), 711.0 ( $b_2$ ), 743.7 ( $a_1$ ), 915.3 ( $b_2$ )
Ta <sub>4</sub> C <sub>4</sub>	-385.1004669	$C_{2v}$	43.5 ( $a_2$ ), 161.8 ( $b_2$ ), 167.0 ( $a_1$ ), 200.1 ( $b_1$ ), 201.3 ( $a_1$ ), 240.5 ( $a_1$ ), 272.3 ( $a_2$ ), 383.4 ( $b_2$ ), 463.8 ( $b_1$ ), 529.8 ( $a_1$ ), 594.3 ( $a_1$ ), 598.2 ( $a_2$ ), 634.3 ( $b_2$ ), 662.3 ( $b_1$ ), 684.4 ( $b_2$ ), 740.8 ( $a_1$ ), 788.9 ( $a_1$ ), 810.3 ( $b_1$ )

**Figure 3.** Calculated structures of (a) Ta<sub>3</sub>C<sub>3</sub> and (b) Ta<sub>3</sub>C<sub>4</sub> overlaid with a cubic framework to show that they form two and three faces, respectively, of a face-centered cube. Shown in (c) is the calculated face-centered cubic structure of Ta<sub>4</sub>C<sub>4</sub>. Note that all Ta–Ta bonds have been removed for clarity.

cluster, Nb<sub>3</sub>C<sub>2</sub>, has been explored with both experimental and theoretical means by Hackett and co-workers.<sup>27</sup> These workers used DFT to identify the two isomers, described above, and referred to them as the triply bonded and doubly bonded isomers, with the former being lower in energy by 0.02 eV. For both the niobium and tantalum analogues, the symmetry of the triply bridged isomer is found to be  $C_{2v}$ , less than the idealized  $D_{3h}$  symmetry due to Jahn–Teller distortion.

In Ta<sub>3</sub>C<sub>3</sub>, we have found that now only one of the carbon atoms sits atop the face of the tantalum triangle and the other two carbon atoms bond along two edges of the triangle, directed away from the first carbon atom (see Table 1). The competition between edge and face bonding seems difficult to rationalize, however, the minimum energy geometry of Ta<sub>3</sub>C<sub>3</sub> is actually a portion of a face-centered cube. When looked at from a different view, the structure forms two faces of a cube, as shown in Figure 3, which is consistent with an overall face-centered cubic structure with two apexes missing. We hypothesize that structures which are building blocks of a face-centered cube are more stable than other geometries.

From the structure shown in Table 1, we see that the optimized geometry of Ta<sub>3</sub>C<sub>4</sub> has a carbon atom sitting atop the triangle face and three carbon atoms bonded to the three edges, directed away from the first carbon atom. Ideally, this structure would have  $C_{3v}$  symmetry, and once again, Jahn–Teller distortion results in a structure with  $C_1$  symmetry. Another structural view, shown in Figure 3, clearly shows that Ta<sub>3</sub>C<sub>4</sub> forms three faces of a cube, which supports the hypothesis that

building blocks of face-centered cubes are the lowest energy structures. A structure corresponding to two face-bonded carbon atoms and two edge-bonded carbon atoms was found to be a transition state at higher energy.

**Ta<sub>4</sub>C<sub>n</sub> Clusters.** The minimum energy geometry of the tantalum tetramer, Ta<sub>4</sub>, forms a “butterfly” structure consisting of a “hinge” and two “wingtips”. The Ta–Ta bond length along the “hinge” is 2.53 Å, whereas the Ta–Ta bond length between the “wingtips” is much larger at 3.28 Å. This structure has already been discussed as being prevalent in condensed-phase organometallic cluster molecules. In terms of our cubic building block hypothesis, the lowest energy minimum would be expected to be a tetrahedron; however, it is obvious that other factors contribute to the breaking of one of the Ta–Ta bonds.

Interestingly, upon the addition of a carbon atom to produce Ta<sub>4</sub>C, the lowest energy geometry is of  $C_s$  symmetry and the distance between the two “wingtip” Ta atoms has now reduced to 2.93 Å. The carbon atom is sitting upon one of the larger faces made up of the two “wingtip” tantalum atoms and one of the “hinge” tantalum atoms. The carbon atom is closer to the two “wingtip” tantalum atoms (1.96 Å) than the third tantalum atom (2.45 Å), which is similar to that seen in Ta<sub>3</sub>C. This geometry is consistent with an overall fcc structure with three apexes missing.

The minimized structure for Ta<sub>4</sub>C<sub>2</sub> shows that the Ta<sub>4</sub> moiety has lost all symmetry, where four of the Ta–Ta bonds are short (2.53, 2.58, 2.59, and 2.59 Å) and two of the Ta–Ta bonds are long (2.86 and 2.89 Å). The carbon atoms now sit on the two larger faces made up of the two “wingtip” tantalum atoms and each of the other “hinge” tantalum atoms. Each carbon atom has a different bond length to the three tantalum atoms that make up each face to produce a molecule with overall  $C_1$  symmetry. Hay and co-workers have reported Hartree–Fock ab initio calculations on Nb<sub>4</sub>C<sub>2</sub> and Nb<sub>4</sub>C<sub>4</sub> using relativistic effective core potentials for the inner atoms of the niobium atom and a double- $\zeta$  valence basis set for all other electrons.<sup>42</sup> For Nb<sub>4</sub>C<sub>2</sub>, they found a geometry with essentially  $C_{2v}$  symmetry corresponding to a bicapped tetrahedron. Using their geometry for Nb<sub>4</sub>C<sub>2</sub> as a starting guess for Ta<sub>4</sub>C<sub>2</sub>, we similarly converged onto a bicapped tetrahedron with  $C_{2v}$  geometry. However, this structure was of higher energy than our  $C_1$  structure and



furthermore, a frequency calculation yielded one imaginary frequency indicating that it is a transition state. Upon relaxing the symmetry to  $C_s$ , the resultant minimum was also shown to be a transition state with one imaginary frequency. Therefore, we have no doubt that the lowest energy structure of  $Ta_4C_2$  is only of  $C_1$  symmetry. Although distorted, this geometry is still consistent with an overall cubic structure having two of its apexes missing.

From the geometry optimization of  $Ta_4C_3$  it seems that the  $Ta_4$  moiety has returned to the “butterfly” structure of  $C_{2v}$  symmetry with a “hinge” bond length being 2.59 Å; however, the “wingtip” has now opened out to 3.75 Å. Two of the carbon atoms sit on the two smaller faces made up of the two “hinge” tantalum atoms and one of the “wingtip” tantalum atoms with bond lengths of 2.10 and 1.98 Å, respectively. The other carbon atom is bonded along the “wingtip” bond, the edge made by the longest Ta–Ta bond. The bond lengths are 1.97 Å from the “wingtip” tantalum atoms and 2.31 Å from the two “hinge” tantalum atoms. Because of the edge bonding of the third carbon atom, this structure is not consistent with an overall cubic structure with a missing apex. It seems that the competition for edge bonding wins out in this situation, contrary to that seen for all other  $Ta_4C_n$  clusters.

The final geometry calculated was that of  $Ta_4C_4$  which we expected to form a face-centered cube consisting of two interpenetrating tetrahedra. This is indeed found, although it is distorted into  $C_{2v}$  symmetry from the idealized  $T_d$  symmetry. The calculation by Hay and co-workers on  $Nb_4C_4$  constrained a structure with  $T_d$  symmetry;<sup>42</sup> however, we could not converge onto a structure constrained to  $T_d$  symmetry. Our calculations show that the  $Ta_4$  moiety is a  $C_{2v}$  “butterfly” with a “hinge” length of 2.45 Å and a “wingtip” length of 2.87 Å. Each carbon atom is in one of two positions which have Ta–C bond lengths of 1.94 and 2.14 Å and 2.02 and 2.07 Å, respectively. However, all four carbon atoms can be considered to be bonded to each of the four faces, and the structure is therefore considered to be a distorted tetrahedron.

#### 4. Conclusions

We have generated a series of neutral tantalum–carbide clusters,  $Ta_mC_n$  ( $m = 1–6$ ,  $n = 1–7$ ), which have been detected as ions following multiphoton ionization. The resulting mass spectra indicate an enhanced stability for  $Ta_4C_n$  clusters. To further explore this, we have undertaken theoretical calculations using density functional theory to characterize the structures of neutral tantalum–carbide clusters,  $Ta_mC_n$  ( $m = 1–4$  and  $n = 0–4$ ). Clusters of the form,  $Ta_4C_n$ , were found to generally build up around a  $Ta_4$  “butterfly” structure with the carbon atoms bonding onto triangular faces made up of three tantalum atoms. This culminates in a distorted  $2 \times 2 \times 2$  face-centered cube of  $C_{2v}$  symmetry for  $Ta_4C_4$ . Clusters containing three tantalum atoms were found to form a triangle, and upon the addition of carbon atoms, there is competition for them to bond to either the face or the edge of the tantalum triangle.

Finally, the appearance of TaO at 355 nm ionization, and not at 532 nm ionization, is postulated to be due to a near-resonant absorption at the first photon step. We intend to explore this further using 1+2 resonance-enhanced multiphoton ionization spectroscopy.

**Acknowledgment.** This work was funded by an Australian Research Council (ARC) Fellowship to G.F.M. and an ARC Large Grant to M.A.B. A Faculty of Science Startup Grant and an ARC Small Grant to G.F.M. are also gratefully acknowl-

edged. Computing resources provided by the South Australian Center for Parallel Computing (SACPC) and The South Australian Computational Chemistry Facility (SACCF) are gratefully acknowledged. G.M.S. is the holder of a University of Adelaide Postgraduate Scholarship. Technical support from the University of Adelaide Mechanical and Electronic workshops and the loan of equipment from the Chemistry Department at the Flinders University of South Australia is also appreciated.

#### References and Notes

- (1) Chupka, W. A.; Berkowitz, J.; Giese, C. F.; Inghram, M. G. *J. Phys. Chem.* **1958**, *62*, 611–614.
- (2) Kohl, F. J.; Stearns, C. A. *J. Phys. Chem.* **1970**, *74*, 2714–2718.
- (3) Kohl, F. J.; Stearns, C. A. *High Temp. Sci.* **1974**, *6*, 284–302.
- (4) Gupta, S. K.; Kingcade, J. E., Jr.; Gingerich, K. A. *Adv. Mass Spec.* **1980**, *8*, 445–451.
- (5) Dietz, T. G.; Duncan, M. A.; Powers, D. E.; Smalley, R. E. *J. Chem. Phys.* **1981**, *74*, 6511–6512.
- (6) Powers, D. E.; Hansen, S. G.; Geusic, M. E.; Pulu, A. C.; Hopkins, J. B.; Dietz, T. G.; Duncan, M. A.; Langridge-Smith, P. R. R.; Smalley, R. E. *J. Phys. Chem.* **1982**, *86*, 2556–2560.
- (7) Michaelopoulos, D. L.; Geusic, M. E.; Hansen, S. G.; Powers, D. E.; Smalley, R. E. *J. Phys. Chem.* **1982**, *86*, 3914–3916.
- (8) McElvany, S. W.; Cassady, C. J. *J. Phys. Chem.* **1990**, *94*, 2057–2062.
- (9) Cassady, C. J.; McElvany, S. W. *J. Am. Chem. Soc.* **1990**, *112*, 4788–4797.
- (10) Guo, B. C.; Kerns, K. P.; Castleman, A. W., Jr. *Science* **1992**, *255*, 1411–1413.
- (11) Guo, B. C.; Wei, S.; Purnell, P.; Buzza, S.; Castleman, A. W., Jr. *Science* **1992**, *256*, 515–516.
- (12) Pilgrim, J. S.; Duncan, M. A. *J. Am. Chem. Soc.* **1993**, *115*, 6958–6961.
- (13) Wei, S.; Guo, B. C.; Purnell, J.; Buzza, S.; Castleman, A. W., Jr. *Science* **1992**, *256*, 818–820.
- (14) Wei, S.; Guo, B. C.; Purnell, J.; Buzza, S.; Castleman, A. W., Jr. *J. Phys. Chem.* **1992**, *96*, 4166–4168.
- (15) Wei, S.; Guo, B. C.; Deng, H. T.; Kerns, K.; Purnell, J.; Buzza, S. A.; Castleman, A. W., Jr. *J. Am. Chem. Soc.* **1994**, *116*, 4475–4476.
- (16) Brock, L. R.; Duncan, M. A. *J. Phys. Chem.* **1996**, *100*, 5654–5659.
- (17) Amrein, A.; Simpson, R.; Hackett, P. *J. Chem. Phys.* **1991**, *95*, 1781–1800.
- (18) Majumdar, D.; Balasubramanian, K. *Chem. Phys. Lett.* **1998**, *284*, 273–280.
- (19) Roszak, S.; Balasubramanian, K. *J. Chem. Phys.* **1997**, *106*, 4008–4012.
- (20) Roszak, S.; Balasubramanian, K. *Chem. Phys. Lett.* **1997**, *265*, 553–560.
- (21) Barnes, M.; Fraser, M. M.; Hajigeorgiou, P. G.; Merer, A. J.; Rosner, S. D. *J. Mol. Spectrosc.* **1995**, *170*, 449–465.
- (22) Johnson, M. A.; Lineberger, W. C. In *Techniques for the Study of Ion–Molecule Reactions*; Farrar, J. M., Saunders, W. H., Eds.; Wiley: New York, 1988.
- (23) Frisch, M. J.; Trucks, G. W.; Schlegel, H. B.; Gill, P. M. W.; Johnson, B. G.; Robb, M. A.; Cheeseman, J. R.; Keith, T.; Petersson, G. A.; Montgomery, J. A.; Raghavachari, K.; Al-Laham, M. A.; Zakrzewski, V. G.; Ortiz, J. V.; Foresman, J. B.; Cioslowski, J.; Stefanov, B. B.; Nanayakkara, A.; Challacombe, M.; Peng, C. Y.; Ayala, P. Y.; Chen, W.; Wong, M. W.; Andres, J. L.; Replogle, E. S.; Gomperts, R.; Martin, R. L.; Fox, D. J.; Binkley, J. S.; Defrees, D. J.; Baker, J.; Stewart, J. P.; Head-Gordon, M.; Gonzalez, C.; Pople, J. *Gaussian 94*, revision E.2; Gaussian: Pittsburgh, PA, 1995.
- (24) Dunning, T. H., Jr.; Hay, P. J. In *Methods of Electronic Structure Theory*; Schaefer, H. F., III, Ed.; Plenum Press: New York, 1976.
- (25) Hay, P. J.; Wadt, W. R. *J. Chem. Phys.* **1985**, *82*, 299–310.
- (26) Yang, D.-S.; Zgierski, M. Z.; Rayner, D. M.; Hackett, P. A.; Martinez, A.; Salahub, D. R.; Roy, P.-N.; Carrington, T., Jr. *J. Chem. Phys.* **1995**, *103*, 5335–5342.
- (27) Yang, D.-S.; Zgierski, M. Z.; Bércecs, A.; Hackett, P. A.; Roy, P.-N.; Martinez, A.; Carrington, T., Jr.; Salahub, D. R.; Fournier, R.; Pang, T.; Chen, C. *J. Chem. Phys.* **1996**, *105*, 10663–10671.
- (28) Yang, D.-S.; Zgierski, M. Z.; Bércecs, A.; Hackett, P. A.; Martinez, A.; Salahub, D. R. *Chem. Phys. Lett.* **1995**, *227*, 71–78.
- (29) Rohlffing, E. A.; Cox, D. M.; Kaldor, A. *Chem. Phys. Lett.* **1983**, *99*, 161–166.
- (30) Rohlffing, E. A.; Cox, D. M.; Kaldor, A. *J. Phys. Chem.* **1984**, *88*, 4497–4502.

- (31) Collings, B. A.; Rayner, D. M.; Hackett, P. A. *Int. J. Mass. Spec. Ion Process* **1993**, 125, 207–214.
- (32) Dyke, J. M.; Ellis, A. M.; Fehr, M.; Morris, A.; Stevens, J. C. H. *J. Chem. Soc. Faraday Trans. 2* **1987**, 83, 1555–1565.
- (33) Ram, R. S.; Bernath, P. F. *J. Mol. Spec.* **1998**, 191, 125–136.
- (34) Premaswarup, D. *Nature* **1955**, 175, 1003–1003.
- (35) Premaswarup, D.; Barrow, R. F. *Nature* **1957**, 180, 602–603.
- (36) Cheetham, C. J.; Barrow, R. F. *Trans. Faraday Soc.* **1967**, 63, 1835–1845.
- (37) Weltner, W., Jr.; McLeod, D. *J. Chem. Phys.* **1965**, 42, 882–891.
- (38) Buntine, M. A.; Stewart, G. M.; Metha, G. F. Manuscript in preparation.
- (39) Cole, S. K.; Liu, K. *J. Chem. Phys.* **1988**, 89, 780–789.
- (40) Simard, B.; James, A. M.; Kowalczyk, P.; Fournier, R.; Hackett, P. A. *Proc. SPIE* **1994**, 2124, 376–387.
- (41) Mingos, M. P.; May, A. S. In *The Chemistry of Metal Cluster Complexes*; Shriver, D. F., Kaesz, H. D., Adams, R. D., Eds.; VCH: New York, 1990.
- (42) Yeh, C. S.; Byun, Y. G.; Afzaal, S.; Kan, S. Z.; Lee, S.; Freiser, B. S.; Hay, P. J. *J. Am. Chem. Soc.* **1995**, 117, 4042–4048.